Feedback of mesoscale ocean currents on atmospheric winds in high-resolution coupled models and implications for the forcing of ocean-only models

Rafael Abel[1], Claus W. Böning[1], Richard J. Greatbatch[1], Helene T. Hewitt[2], and Malcolm J. Roberts[2]

[1]GEOMAR Helmholtz Centre for Ocean Research Kiel, Kiel, Germany
[2]Met Office, Exeter, United Kingdom

Correspondence to: Rafael Abel, rabel@geomar.de

Abstract. The repercussions of surface ocean currents for the near-surface wind and the air-sea momentum flux are investigated in two versions of a global climate model with an eddying ocean. The focus is on the effect of mesoscale ocean current features at scales of less than 150 km, by considering high-pass filtered, monthly-mean model output fields. We find a clear signature of a mesoscale oceanic imprint in the wind fields over the energetic areas of the oceans, particularly along the extensions of the western boundary currents and the Antarctic Circumpolar Current. These areas are characterized by a positive correlation between mesoscale perturbations in the curl of the surface currents and the wind curl. Coupling coefficients between the curl of the surface currents and the wind curl are estimated using linear regression. The coupling coefficients are spatially non-uniform and show a pronounced seasonal cycle. The positive feedback of mesoscale current features on the near-surface wind acts in opposition to ~~their~~ the current-induced damping effect on the ~~wind stress.~~ surface stress. The current-wind feedback thus reduces the well-known damping of mesoscale eddies by the current-stress interaction that is typically accounted for by the usage of 'relative winds' in the stress-formulation of many models. A tentative incorporation of this feedback in the surface stress formulation of an eddy-permitting global ocean-only model leads to a ~~gain in the kinetic energy of up to 10, suggesting a fundamental shortcoming of present ocean model configurations.~~ more accurate mechanical surface coupling when comparing to coupled simulations.

1 Introduction

During the last decade, studies of satellite observations and high-resolution coupled ocean-atmosphere models have revealed some intriguing impacts of mesoscale ocean fronts and eddies on the near-surface winds. Spurred by the identification of an imprint on the surface wind of gradients in sea surface temperature (SST) associated with meandering oceanic fronts (*Xie*, 2004; *Chelton et al.*, 2004), a particular emphasis of research has been on the mechanisms of the thermal air-sea coupling. At mid-latitudes, air-sea interaction at larger scales ~~shows~~ exhibits a negative correlation between SST anomalies and surface wind, reflecting a passive role of the ocean in atmospheric forcing (e.g. Mantua et al., 1997; Okumura et al., 2001) . The interaction is reversed at smaller spatial scales where SST anomalies exert an influence on wind speeds and surface stress via perturbations of the atmospheric boundary layer (*Wallace et al.*, 1989; *Samelson et al.*, 2006; *Spall*, 2007; *Small et al.*, 2008),

leading to a positive SST - wind stress correlation for quasi-stationary frontal regions (*Bryan et al.*, 2010; *Roberts et al.*, 2016) and transient eddies (*Frenger et al.*, 2013). The It is well established that the SST - wind (stress) coupling can have important repercussions for tropospheric weather patterns (*Minobe et al.*, 2008), while in turn, the damping of SST anomalies by enhanced winds constitutes a negative feedback on the oceanic mesoscale (*Shuckburgh et al.*, 2011)that represents a dominant
5 factor in; while thermal heat fluxes due to mesoscale SST anomalies have important implications for the energetics of western boundary currents (*Ma et al.*, 2016).

Another aspect of mesoscale air-sea coupling concerns the imprint of surface currents. It has long been recognized that current-induced vertical velocity shear shear in the horizontal velocities at the ocean's surface can influence frictional air-sea
10 coupling and thus can cause surface motions to decay (*Dewar and Flierl*, 1987; *Pacanowski*, 1987). Accounting for the ocean surface current in the surface stress formulation used in ocean circulation models, i.e. the use of 'relative winds' across the interface instead of 'absolute winds' in the bulk parameterization of the turbulent momentum flux, was found to significantly (up to 30%) reduce the energy input to the large-scale circulation (*Duhaut and Straub*, 2006; *Zhai and Greatbatch*, 2007; *Hughes and Wilson*, 2008; *Scott and Xu*, 2009) and by up to 70% in the near-inertial frequency band (*Rath et al.*, 2013). In eddying models
15 the eddy kinetic energy (EKE) was found to be reduced (*Zhai and Greatbatch*, 2007; *Seo et al.*, 2016) due to increased surface drag (*Eden and Dietze*, 2009) and reduced wind energy transfer (*Hutchinson et al.*, 2010), with implications for primary production (*Eden and Dietze*, 2009). Compared to the thermal interaction via mesoscale SST anomalies, the mechanical damping via the current-surface stress coupling was found to be much more dominant for the dynamics of the mean and eddy currents in a regional model study (*Seo et al.*, 2016). In contrast *Byrne et al.* (2016) report that in regions with strong wind gradients
20 like the Antarctic Circumpolar Current (ACC), the thermal effect outweighs the mechanical effect with respect to the EKE of vortices and their lifetimeIn a regional model study it was shown that for the surface stress formulation, the effect of mesoscale current anomalies was much more important that the effect of mesoscale SST anomalies (*Seo et al.*, 2016). Regionally the large-scale wind curl is quite important for the wind power input to mesoscale features: When the large-scale wind curl has the same sense of rotation as the eddies it spins up the eddies; if the senses of rotation have opposing signs eddies are spun down
25 (Xu et al., 2016; *Byrne et al.*, 2016). Thermal effects due to mesoscale SST anomalies influence the boundary layer above, which induces changes in the winds and therefore may also alter spin up and spin down effects (*Byrne et al.*, 2016).

While previous work on the role of surface currents in the air-sea momentum transfer focused on the effect of surface stress changesfor the energetics of the ocean, recent studies also began to consider the their implications for the near-surface winds.
30 *Moulin and Wirth* (2016) investigated the local exchange of momentum between idealized turbulent layers of ocean and the ocean and the atmosphere at the scale of ocean eddies, showing that owing to the large difference in inertia between the two components, the atmosphere can be influenced by persistent ocean features, while its short time fluctuations tend to be independent of the ocean dynamics. *Renault et al.* (2016b) investigated the influence of mesoscale ocean eddies on the momentum exchange in a regional high-resolution coupled ocean-atmosphere model of the California Current System (CCS). They showed
35 that the current feedback can conceptually be split into two parts: its effect on the surface stress which induces a damping on the

~~EKE~~surface currents, and a ~~subsequent~~ concomitant effect on the near-surface winds which partly counteracts the damping and re-energizes the atmosphere (and subsequently the ocean). They found that the near-surface winds are enhanced by about 20% of the surface ocean current. Based on their findings for the CCS, *Renault et al.* (2016b) suggest that for uncoupled ocean-only models, the partial re-energisation should be taken into account in the bulk formulae of the wind stress.

5

This study extends the approach of *Renault et al.* (2016b) by examining the air-sea momentum transfer at the oceanic mesoscale in two versions of a global climate model with 'eddy-permitting' and 'eddy-resolving' ocean components. More specifically, ~~we use the coupled model simulationsto~~ using the coupled simulations, our objectives are (1) to identify the imprint, including its spatial distribution, of mesoscale ocean current features on the near-surface winds over the global ocean by inspecting spatially high-pass filtered surface currents and near-surface winds; (2) to investigate its repercussion for the surface momentum flux, i.e., the effect of the current - wind feedback on the current - surface stress relation~~;~~. Using an ocean-only model set-up, we also (3) ~~to~~ give a preliminary assessment of ~~its potential impacts for~~ the potential impact of the coupling between the ocean surface velocity and the near-surface winds on the mean and eddy kinetic energies of an eddy-permitting global ocean model~~,~~. We do this based on a tentative implementation of the diagnosed spatially-variable, monthly-mean distribution of the current-wind coupling in the bulk surface stress formulation and show that this approach is surprisingly good at reproducing the mechanical coupling seen in the fully coupled models.

2 Methods & Models

2.1 Methods

Both atmospheric surface winds and ocean-surface currents determine the surface stress

$$\boldsymbol{\tau} = \rho_a C_D |\boldsymbol{U} - \alpha\boldsymbol{u}|(\boldsymbol{U} - \alpha\boldsymbol{u}), \tag{1}$$

where ρ_a is air density, C_D the drag coefficient~~(note that C_D also depends on the choice of α as $|\boldsymbol{U} - \alpha\boldsymbol{u}|$ is used for the calculation)~~, $\boldsymbol{U}$ the 10m wind , $\boldsymbol{u}$ the ocean surface current and α a parameter representing the influence of ocean currents. (Since C_D is also function of the relative velocity $\boldsymbol{U} - \alpha\boldsymbol{u}$ and the surface stability, it also depends on the choice of α.) Note that we chose to use the wording 'surface stress' instead of the more commonly used 'wind stress' as the stress is not entirely determined by the wind. Since the wind speed is typically an order of magnitude larger than the ocean current speed, ~~the challenge is~~ it is a challenge to detect the imprint of ocean currents ~~in~~ on the surface stress. Fortunately the inherent spatial and temporal scales of the atmosphere and the ocean are very different. While at mid-latitudes atmospheric mesoscale variability is typically associated with time scales of hours to days and spatial scales of hundreds to thousands of kilometers, the oceanic variability is most energetic at time scales of days to weeks with spatial scales of tens of kilometers.

30   For assessing the imprint of the oceanic variability, we use monthly-mean model output from coupled atmosphere-ocean and forced ocean-only simulations and apply a spatial Hann-type high-pass filter to remove variability on scales longer than

approximately 150km (see Appendix A for discussion of this choice and associated sensitivities). Model output closer than 150km to the coast is ~~neglected~~ not used as orographic and coastline effects may also introduce small-scale distortions to the wind field (*Perlin et al.*, 2007; *Renault et al.*, 2016a).

5 The smallest spatial scales present in the data are emphasized further by considering the curl of the wind, of the surface stress, and of the ocean surface currents in the quantification of the current-wind and current-stress ~~linkage. Assuming~~ linkages. Here we assume a linear relationship in the form

$$curl(\boldsymbol{U})\underline{10^2} = s_{\underline{st}\,w}\,curl(\boldsymbol{u}) \tag{2}$$

$$curl(\boldsymbol{\tau})\,\underline{10^2} = s_{\underline{w}\,st}\,curl(\boldsymbol{u}), \tag{3}$$

where the coupling coefficients $s_{\underline{st}}$ ~~and~~ s_w and s_{st} are estimated by linearly regressing the ~~stress curl /wind~~ curl ~~as a function of the oceanic current vorticity~~ of the near-surface wind and the curl of the stress, respectively, against the vorticity of the ocean

10 currents. We note that other studies used bin averaging for the same quantities (*Renault et al.*, 2016b), and for the relationship between the SST gradient and the wind curl or wind gradient (*Chelton et al.*, 2007); however, a bin averaging was ~~not found~~ found not to be necessary here. Note also that the factor 10^2 is simply used to get coupling coefficients of O(1).

As a means to account for the partial re-energisation of the near-surface winds in the atmospheric forcing of uncoupled

15 ocean models, *Renault et al.* (2016b) proposed to tweak the bulk formulation of the surface momentum flux by using (1) with $\alpha = 1 - s_w$. From their regional model results *Renault et al.* (2016b) estimated an $s_w = 0.23 \pm 0.01$ for the CCS. We extend this approach here by estimating the spatial distribution of the coupling coefficient s_w from two global coupled simulations. We then proceed to test the ~~suggestion of *Renault et al.* (2016b) by forcing a set~~ sensitivity of global ocean-only simulations, to the suggestion of *Renault et al.* (2016b) using (1) with a spatially-varying parameter α in comparison to the classical 'absolute

20 wind' and 'relative wind' forcing formulation.

2.2 Models

The ~~coupled~~ analysis related to our objectives (1) and (2) uses output from the eddying climate model experiments GC2-N512 (hereafter C1/4) and GC2.1-N512O12 (hereafter C1/12), that employ the atmospheric Met Office Unified Model at N512 resolution (~~$\sim 25km$~~ $\sim$ 25km) and ocean components based on Nucleus for European Modelling of the Ocean (NEMO;

25 *Madec*, 2011) ORCA025 and ORCA12, with a nominal resolution of $1/4°$ and $1/12°$, respectively. Turbulent surface fluxes are calculated using a bulk formulation (*Smith*, 1988) with Charnock's coefficient of 0.018, ~~with~~ using relative winds ($\alpha = 1$) and coupling frequencies of 3-hourly ~~(~~for C1/4 ~~)~~ and 1-hourly ~~(~~for C1/~~12).~~12. The atmospheric model has 85 vertical levels (Appendix D). Unresolved turbulent motions are parametrized to achieve realistic vertical structures in temperature and wind profiles (Walters et al., 2017) . For an extensive documentation of the model configurations and a discussion of the impacts

30 of a resolved ocean mesocale in the simulations we refer to *Hewitt et al.* (2016). A discussion of the impact of the oceanic mesoscale on the thermal air-sea interaction, i.e. the SST - surface stress relationship, has been given by *Roberts et al.* (2016).

Here we consider the interaction due to momentum transfer at the oceanic mesoscale. The models were integrated for 19 years (year 20 experienced some data loss) ~~,~~ and the last 15 years are used for the analysis. Even if 20 year runs might be too short for the deep ocean to spin up, they are sufficient for the surface coupling investigated in this study.

5 ~~The~~ In order to obtain a preliminary assessment of the potential impacts of the current-wind coupling in an eddying ocean-only ~~experiments are~~ model, we ran a sequence of experiments with a standard eddy-permitting model (ORCA025). The model is based on NEMO (version 3.4) ~~in an ORCA025 configuration. This configuration~~ and uses a tripolar grid at a nominal resolution of $1/4°$, and 46 vertical levels with a resolution of 6m near the surface and 250m at depth. Surface-forcing fields build on the interannually varying Coordinated Ocean-Ice Reference Experiments ~~(CORE, *Large and Yeager*, 2009; *Griffies et al.*, 2009)~~

10 (COREv2, *Large and Yeager*, 2009; *Griffies et al.*, 2009) and have a temporal resolution of 6 hours and a spatial resolution of $2°$ that is interpolated on the model grid. Turbulent air-sea fluxes are calculated using the bulk formulae given by *Large and Yeager* (2004). The ~~experiments~~ simulations were started from a 30-yr spinup (1980-2009), which was initialized with the World Ocean Atlas 1998 (*Antonov et al.*, 1998; *Boyer et al.*, 1998) and then carried out through 1989-2004. Four forced experiments were performed: with absolute winds ($F_{\alpha=0}$), relative winds ($F_{\alpha=1}$), and two experiments that use spatially and

15 temporally variable α given by the distribution of the coupled experiments C1/4 ($F_{\alpha=C1/4}$) and C1/12 ($F_{\alpha=C1/12}$). ~~Further details are given in the next section.~~ The analysis uses the last 15 years of each integration.

3 Results

3.1 Ocean current feedback on near-surface winds

Generally the momentum exchange between ~~atmosphere and~~ the atmosphere and the ocean is from the atmosphere to the

20 ocean. ~~In forced ocean models we find that for high-pass filtered data there is no relation between the curl of the surface current and the curl of the~~ Here we show that on small spatial scales the ocean surface currents can excite anomalously near-surface winds ~~(Fig. 1 a)~~. In coupled models, the surface stress also acts as the bottom boundary condition for the ~~atmospheric models~~ atmosphere and thus has an impact on the near-surface winds. ~~In contrast to the forced ocean-only simulations, the coupled simulations thus bear~~ This gives rise to a relation between the curl of the ocean currents and the curl of the wind over energetic

25 oceanic regions such as the Gulf Stream Extension (Fig. 1~~b,c)~~ a,b) in coupled simulations, reflecting an influence of intense mesoscale ocean currents on the ~~surface~~ near-surface wind. The slope of the linear regression of both quantities gives the coupling coefficient for the wind (s_w). Both coupled experiments, C1/4 ($s_w = 0.48 \pm 0.05$) and C1/12 ($s_w = 0.47 \pm 0.03$), yield similar estimates for the coupling coefficient, here shown for the month of June. In uncoupled ocean models such a relation is not found (Fig. 1c) confirming that on small spatial scales the surface currents drive the winds and not the other way around.

30

The influence of ocean surface currents ~~to~~ on near-surface winds does show a strong spatial variability. Therefore s_w is estimated in $2°x2°$ boxes over the global ocean. The largest mean values of s_w (up to 0.5) are found over the Western Boundary Current Extension (WBCE) regions and the ACC, while in less energetic regions the s_w values tend to be smaller (Fig. 2; note
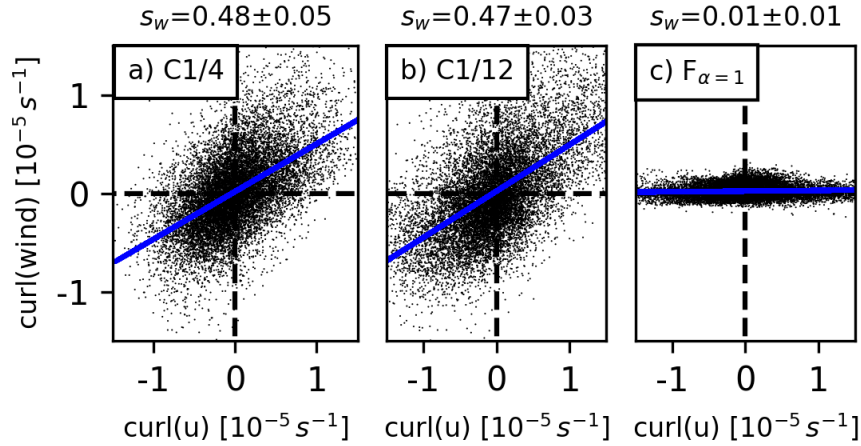
5

Figure 1. Influences on near-surface (10m) winds by mesoscale ocean surface currents~~and its dependence on atmospheric stability~~. Relation between curl(u) and curl(wind) with linear regression (blue) at the Gulf Stream (GS) Extension (35-45°N, 62-72°W) for the coupled models (a) ~~$F_{\alpha=1}$, (b)~~ C1/4 and (~~e~~b) C1/12, and for the standard forcing configuration ('relative winds') in an uncoupled model (c) $F_{\alpha=1}$ for June. Note that also for the 'absolute wind' configuration ($F_{\alpha=0}$) no relation is found. The slope of the linear regression (s_w) is shown at the top. The standard error of the slope is calculated employing a binomial method (see Appendix C).

that in weakly-energetic regions like the subtropics the method fails to diagnose a robust relationship, for more details we refer to Appendix B)~~, while in less energetic regions the s_w values tend to be smaller~~. Both coupled experiments C1/4 and C1/12 show a similar pattern~~, with somewhat smaller values in C1/12.~~.

5   It is fair to assume that the impact of the ocean surface currents on the near-surface wind depends on the ~~condition~~ state of the atmospheric boundary layer. Accordingly, the coupling coefficient s_w shows a strong seasonal cycle in both coupled experiments, with larger values in summer than in winter (Fig. 3a): e.g., the values are up to 0.5 in summer and values of 0.2 in winter over the Gulf Stream Extension. The general behaviour is similar in both coupled experiments, with some quantitative differences in the amplitudes of s_w. Over the ACC (Fig. 3b) almost no seasonal cycle is found with $s_w \approx 0.35$ (C1/4) and
10   $s_w \approx 0.31$ (C1/12).

    The seasonality in the coupling coefficient and the different behaviour between GS and ACC regimes can be rationalized in terms of the stability of the near-surface atmosphere, as given by the vertical temperature gradient between the first two levels of the atmospheric model, 20m and 53m, (Fig. 3 red curves). The relationship between the atmospheric stability and the
15   coupling coefficient s_w suggests that the influence of the ocean surface currents is spread over a deeper atmospheric layer when its stability is weak. More specifically, for the GS region, cold winds from the continent during winter lead to strong turbulent heat fluxes over the Gulf Stream that destabilize the near-surface atmosphere, reflected by a negative vertical temperature
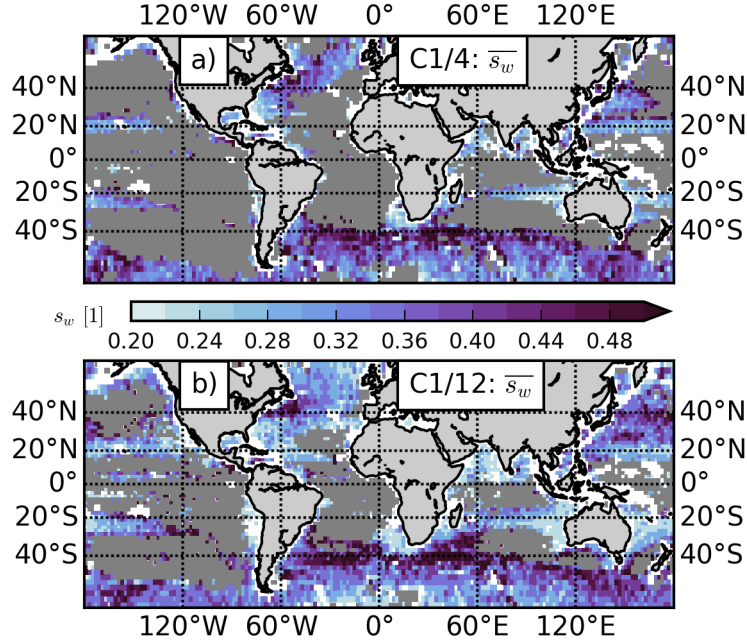
Figure 2. Mean of s_w monthly values for (a) C1/4 and (c) C1/12. Note that the last 15 years of the simulations are used for the analysis. Grey shading denotes areas where the curl of the ocean currents is too small so that the estimates of s_w are biased to too large values (see Fig. A2).

gradient. This implies that the partial re-energisation of the winds (due to the presence of ocean currents) in winter happens over a deeper layer than during summer when the near-surface atmosphere is stable (positive vertical temperature gradient). Accordingly the change in the near-surface wind is smaller in winter as the gain of momentum is distributed over a deeper layer, resulting in a smaller s_w than in summer. During summer months the near-surface layers are relatively shallow which

5   leads to stronger changes in near-surface winds due the presence of ocean currents, i.e. larger s_w. While the amplitude of the seasonality is similar in the north-western Pacific (Kuroshio regime), it is much smaller in the ACC regime where the monthly mean vertical temperature gradients are always positive, resulting in a large mean s_w and very little seasonal variability (Fig. 4). The lack of a seasonality in the near-surface stability of the atmosphere also results in low correlation between the stability and s_w.
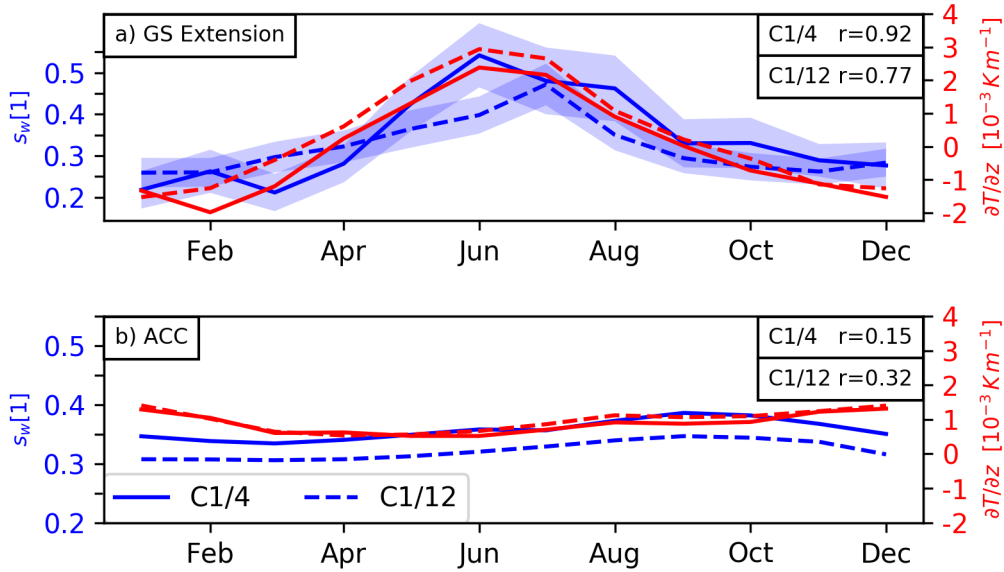
10

Figure 3. Seasonal cycle of coupling coefficient s_w (blue) and vertical temperature gradient between the first two model levels (red) T(53m) minus T(20m) for (a) GS Extension and (b) the ACC (80-40°S); C1/4 (solid) C1/12 (dashed). Correlation coefficients (r) between the coupling coefficient s_w and the vertical temperature gradient are shown at the upper right for the different experiments and regions. Blue shading denotes the standard error of the slope and is calculated employing a binomial method (see Appendix C). For b) the error is of equivalent magnitude, but not shown for visibility reasons.

The strength of the seasonal cycle of s_w does vary with region. An illustration of the spatial distribution of the amplitude is given in Fig. 4, ~~showing~~ which shows the temporal standard deviation of the monthly-mean values of s_w. The main pattern is the contrast between the strong seasonality of the northern hemisphere WBCs and the core of the ACC reflecting the different seasonality in the stability of the near-surface atmosphere. This is emphasized in Fig. 5, showing the correlation between the variability of s_w and near surface stability ($\partial T/\partial z$).

The stability of the near-surface atmosphere tends to determine the strength of the coupling coefficient s_w. Over the WBCE regions the variability of the near-surface stability is high and with that the variability of the coupling coefficient s_w is also high. Positive correlations in Fig. 5 illustrate that relation. For the WBCE of the Gulf Stream, the Kuroshio, the Malvinas, as well as for the CCS and the tropical and the subtropical oceans (i.e., for those parts not greyed out), the correlations are positive indicating a relation between the near-surface stability and the coupling parameter s_w. For most of the Southern Ocean ~~the signal is small and ambiguous, with alternating positive and negative correlations~~positive correlations are found. However, in some regions the correlations found are not significant at a 90% level which might be due to other processes that superimpose
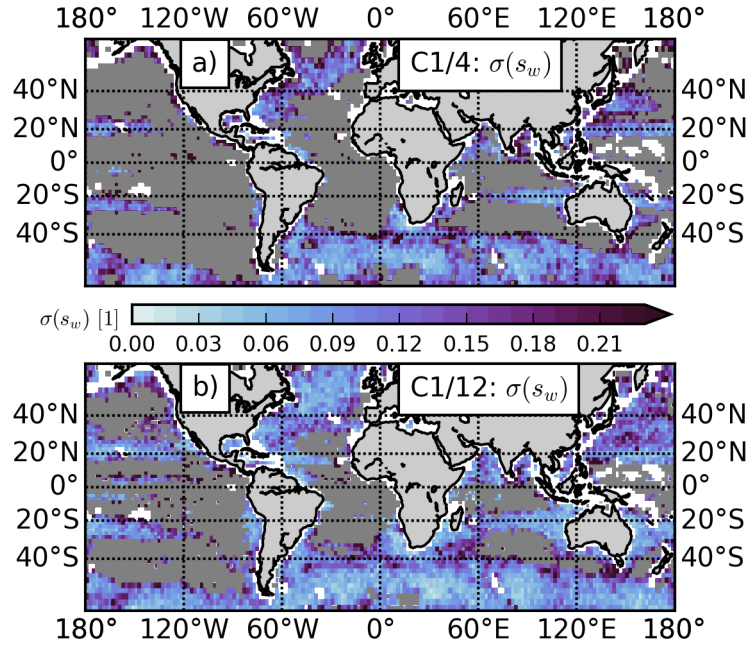
Figure 4. Standard deviation of s_w monthly values for (a) C1/4 and (c) C1/12. Grey areas defined as in Fig. 2.

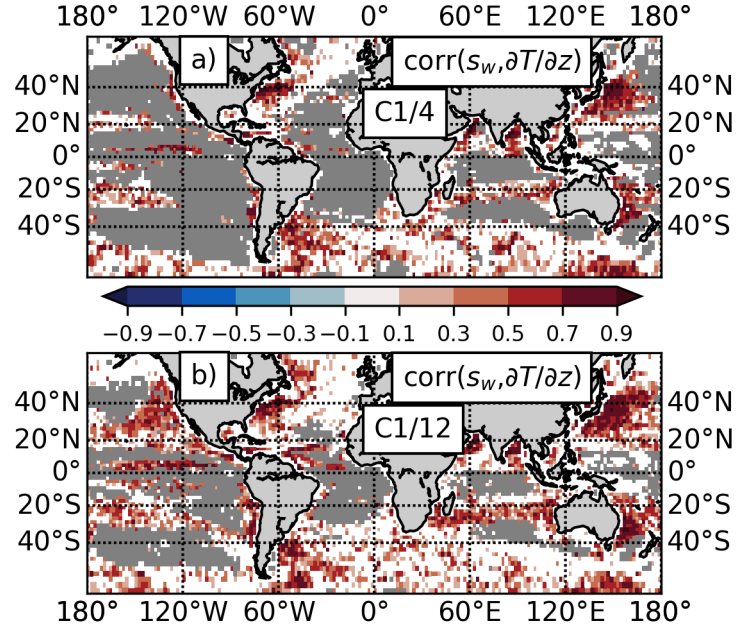the relation between the near-surface stability and the coupling coefficient s_w. A coherent negative patch is

Figure 5. Correlation between the coupling coefficient s_w and near surface stability between the first two model levels ($\partial T/\partial z$) for (a) C1/4 and (b) C1/12. Positive correlations reflect that in unstable conditions low s_w values are found and in stable conditions high s_w values are found. Only p values smaller than 0.1 are considered. Grey areas defined as in Fig. 2.

3.2 Imprint of ocean surface currents on the surface stress

The presence of ocean surface currents is accounted for in the surface stress formulation (1). The strength of the coupling can be expressed by the coupling coefficient s_{st} which is estimated by the slope of the linear regression between the curl of the ocean surface currents and the curl of the surface stress. The more negative s_{st} the stronger the coupling and the damping of surface currents. In the Gulf Stream Extension region we find large values of s_{st} up to -3 in winter and smaller values as low as -1 in the summer consistently in both coupled simulations, indicating stronger damping in summer than in winter (Fig. 6). The coupling strength is largely determined by the drag coefficient C_D which is to leading order a function of the background wind. We find that the background wind has a maximum in winter and a minimum in summer which results in negative correlations with s_{st} of the order of $r = -0.6$. Over the ACC the background winds are stronger but the temporal variability is less pronounced which results in stronger coupling coefficients s_{st} with less temporal variability and correlation coefficients of similar magnitude compared to the Gulf stream extension.
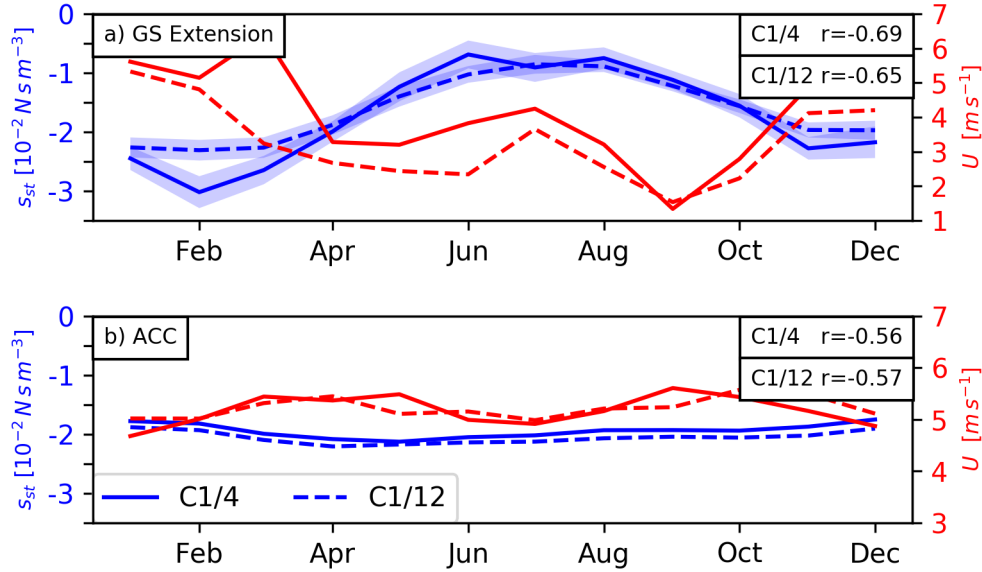
Figure 6. Seasonal cycle of coupling coefficient s_{st} (blue) and monthly mean background wind speed U (red) for (a) GS Extension and (b) the ACC ($80\text{-}40°$S); C1/4 (solid) C1/12 (dashed). Correlation coefficients (r) between the coupling coefficient s_w and the background wind speed U are shown at the upper right for the different experiments and regions. Blue shading denotes the standard error of the slope and is calculated employing a binomial method (see Appendix C). For b) the error is of equivalent magnitude, but not shown for visibility reasons.

In a global perspective the coupling coefficient s_{st} has a strong spatial variability consistently found in both coupled simulations (Fig. 7). Large mean s_{st} values up to -3 are found over the ~~eastern North Atlantic . This however, is an area with small coupling coefficients s_w and relatively small ocean currents, it could thus be close to the detection limit discussed in Appendix A~~Gulf Stream extension region, the Kuroshio extension region and the ACC in particular in the Atlantic and Indian

5   Ocean sectors. These areas are commonly associated with strong winds. Regions with small s_{st} are mostly equatorward from $40°$N and S and have typically much smaller background winds than in the westerly wind regions. The patterns of C1/4 and C1/12 are surprisingly similar indicating only a minor influence from the horizontal resolution.

The relation between the coupling coefficient s_{st} and the background wind holds in most regions as indicated by negative correlations (Fig. 8) with large negative correlation over the Gulf Stream and Kuroshio extension, large areas in the Southern

10 Ocean, the Indian Ocean and other subtropical regions. However, in some regions the correlations found are not significant at a 90% level which might be due to other processes that superimpose on the relation between background wind speed and the coupling coefficient s_{st}.
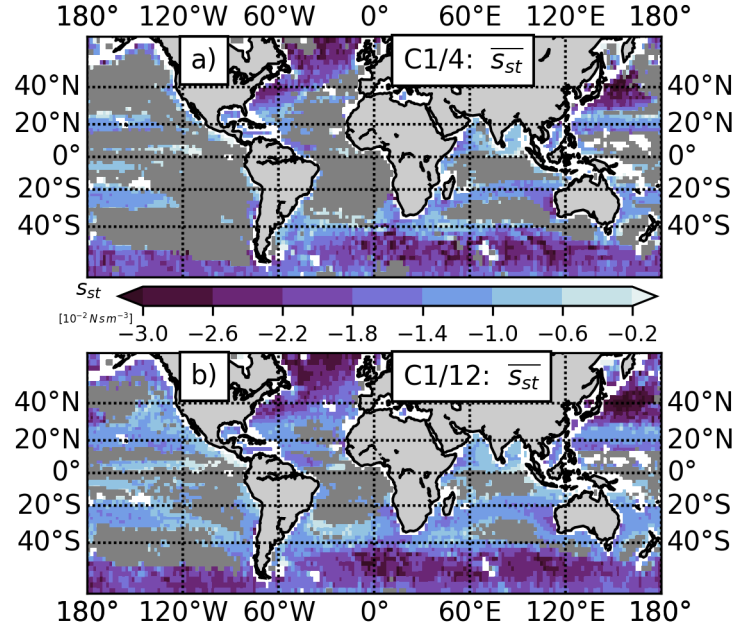
Figure 7. Mean of s_{st} DJF monthly values for (a) C1/4 and (c) C1/12. Grey areas defined as in Fig. 2.

~~The effect of the partial re-energisation of the atmospheric winds~~ We use s_{st} as a measure of the fidelity of the momentum flux representation and illustrate the coupling coefficients for C1/4, C1/12, $F_{\alpha=0}$, and $F_{\alpha=1}$ for the Gulf Stream Extension in the month of January in Fig. 9. In comparison to the s_{st}-values for the coupled models (-2.23 ± 0.05 for C1/4 and -2.26 ± 0.05 for C1/12), the coefficient in the relative wind simulation ($F_{\alpha=1}$) indicates a much too strong effect ($s_{st} = -3.28\pm0.03$), whereas there is no coupling in the absolute wind simulation ($F_{\alpha=0}$, $s_{st} = 0.04\pm0.03$).

This discrepancy in the coupling coefficient s_{st} between the forced and coupled simulations is not due to different background winds, but due to the ~~influence of ocean surface currents in the surface stress estimation is missing in the forcing formulation currently used for ocean-only models .~~ missing re-energization of atmospheric winds. As we showed in the previous section this re-energization is present in the coupled simulations and excites a curl in the wind that has the same sense of rotation as the curl of the ocean current. This re-energization therefore effectively reduces the damping of surface currents and leads to smaller coupling coefficients s_{st}. As this mechanism is missing in forced ocean models the coupling coefficients tend to be too large $F_{\alpha=1}$. In the following we test the sensitivity of a forced model to an implementation of the re-energization suggested by *Renault et al.* (2016b) .
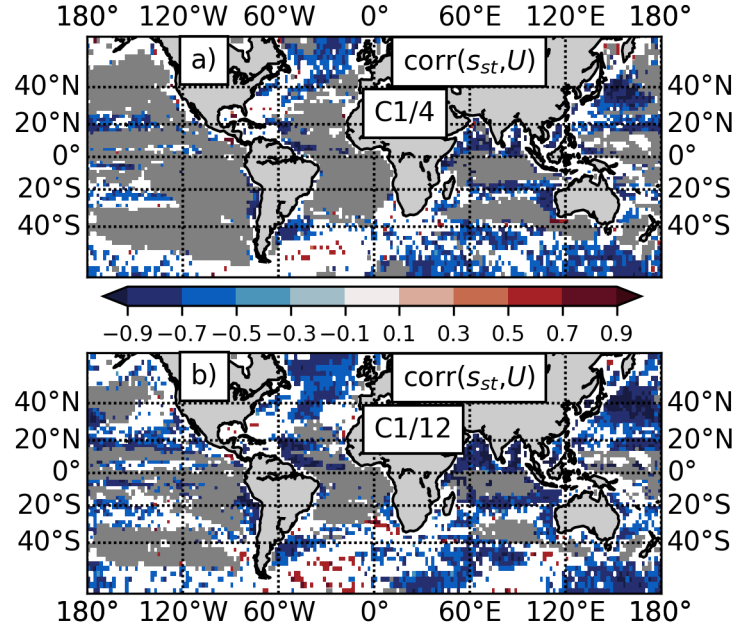
Figure 8. Correlation between the coupling coefficient ~~s_w~~ $s_s t$ and ~~near surface stability ($\partial T/\partial z$)~~ background wind speed U for (a) C1/4 and (b) C1/12. ~~Positive~~ Negative correlations reflect that ~~in unstable~~ under strong wind conditions ~~low s_w~~ large negative s_{st} values are found and ~~in stable~~ that for low wind conditions ~~high s_w~~ small s_{st} values are found. Only p values smaller than 0.1 are considered. Grey areas defined as in Fig. 2.

3.3 Preliminary assessment of the re-energization effect tentatively implemented in uncoupled models

In the previous sections we showed that in coupled atmosphere ocean models, the near-surface winds get re-energized by the surface currents. In uncoupled ocean models such a mechanism is missing due to the fact that the atmospheric state is specified. One consequence of this deficiency is a too strong damping of surface currents in uncoupled ocean models in the

5   'relative wind' configuration. As a correction *Renault et al.* (2016b) suggest to modify the velocity used in the bulk formulation (1) by $U + s_w \cdot u - u$, so that the wind U is re-energised by $s_w \cdot u$, where u is the ocean current velocity. We then use $\alpha = 1 - s_w$ in (1) to force ocean-only models. As a test of its potential use in forced ocean-only models, following the suggestion of *Renault et al.* (2016b), a monthly-varying climatology of s_w is calculated from C1/4 and C1/12 with $2° \times 2°$ resolution, and used in (1) with $\alpha = 1 - s_w$. For the areas with grey shading in Fig. 2 the global mean values of $\alpha = 0.65$ (C1/4) and $\alpha = 0.69$ (C1/12) are applied. The bulk forcing with this α ($F_{\alpha=C1/4}, F_{\alpha=C1/12}$) is used as part of a series of ocean-only experiments. ~~In the~~

10   ~~following sections we assess how well these experiments perform with respect to the coupled experiments.~~
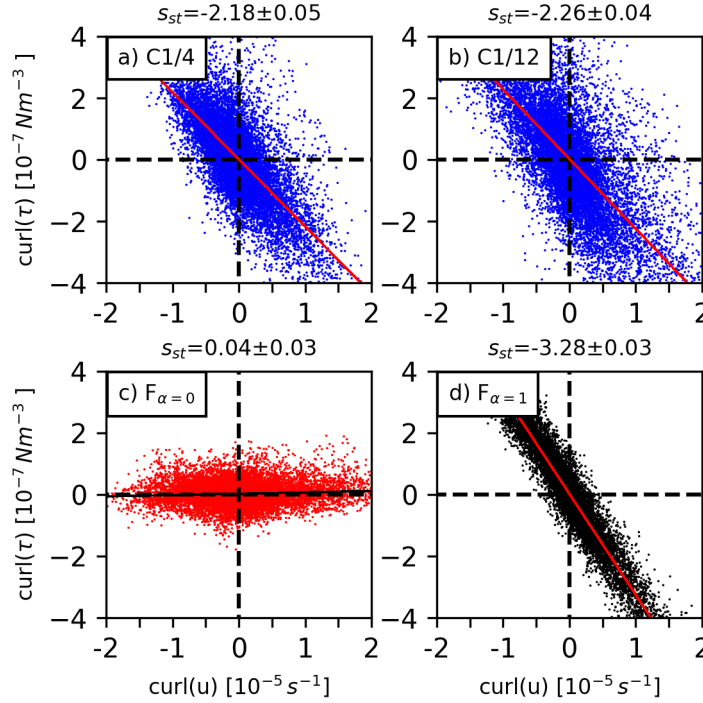
13

Figure 9. Ocean-surface current and surface stress coupling coefficient s_{st} for (a) C1/4 (blue), (b) C1/12 (blue), (c) $F_{\alpha=0}$ (red), and (d) $F_{\alpha=1}$ (black), over the Gulf Stream Extension (35-45°N, 62-72°W) for January. Linear regressions are depicted by solid lines; slopes and errors of the slopes are shown in the titles.

3.4 ~~Imprint of ocean surface currents on the surface stress~~

~~The presence of ocean surface currents is accounted for in the surface stress formulation (1). The strength of the coupling can be expressed by the coupling coefficient s_{st} which is estimated by the slope of the linear regression between the curl of the ocean surface currents and the curl of the surface stress. The more negative s_{st} the stronger the coupling. We use s_{st} as~~ a measure of the fidelity of the momentum flux representation in the eddy-permitting, forced ocean simulations, using $\alpha=0$ ($F_{\alpha=0}$), $\alpha=1$ ($F_{\alpha=1}$) and a spatially-varying field of α obtained from the coupled simulation ($F_{\alpha=C1/4}$, $F_{\alpha=C1/12}$). The results are illustrated for the Gulf Stream Extension in the month of January in Fig. 9 (C1/12 is not shown). In comparison to the s_{st}-values for the coupled models (-2.23 ± 0.05) for C1/4 and -2.26 ± 0.05 for C1/12), the coefficient in the relative wind simulation ($F_{\alpha=1}$) indicates a much too strong effect ($s_{st}=-3.28\pm0.03$), whereas there is no coupling in the absolute wind simulation ($F_{\alpha=0}$, $s_{st}=0.04\pm0.03$). However, when modifying the bulk formulation by using the global distribution of α-values obtained above, the forced ocean-only experiments were able to produce coupling coefficients $s_{st}=-2.42\pm0.03$ ($F_{\alpha=C1/4}$) ~~and $s_{st}=-2.44\pm0.03$ (~~: $s_{st}=-2.42\pm0.03$ and $F_{\alpha=C1/12}$: $s_{st}=-2.44\pm0.03$) that are close to the estimates

14

$s_{st}=-2.42\pm0.02$ $s_{st}=-2.44\pm0.02$

d) $F_{\alpha=C1/4}$ d) $F_{\alpha=C1/12}$

curl(τ) [$10^{-7}\,Nm^{-3}$]

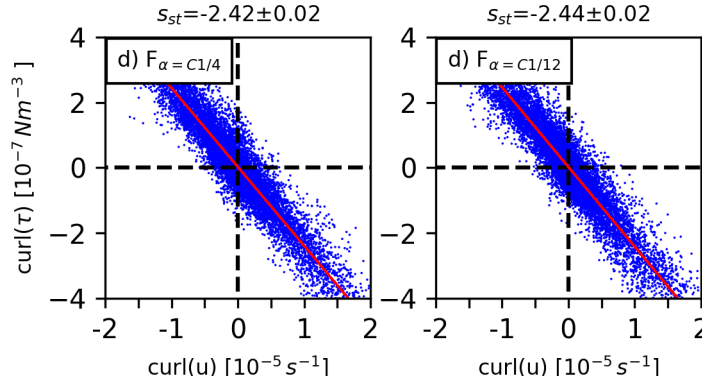curl(u) [$10^{-5}\,s^{-1}$] curl(u) [$10^{-5}\,s^{-1}$]

Figure 10. Ocean-surface current and surface stress coupling coefficient s_{st} for (a) F~~$_{\alpha=1}$~~ $_{\alpha=C1/4}$, (b) F~~$_{\alpha=1}$, (c) F$_{\alpha=C1/4}$~~ (blue), and (d) ~~C1/4~~ $_{\alpha=C1/12}$ over the Gulf Stream Extension (35-45°N, 62-72°W) for January. Linear regressions are depicted by solid lines; slopes and errors of the slopes are shown in the titles.

of the coupled experiments (Fig. 10). This implies that the surface stress (or 'top drag') experienced by mesoscale ocean features is of comparable strength in C1/4, C1/12, $F_{\alpha=C1/4}$, $F_{\alpha=C1/12}$, demonstrating that forced simulations with the partial re-energisation tweak proposed by *Renault et al.* (2016b) ~~is bringing the forced experiments closer to~~ produce comparable coupling coefficients as the fully coupled ~~experiments~~simulations, at least in the Gulf Stream Extension region. Differences in 5 the near-surface atmospheric state like the background wind speed and bulk algorithms are likely to account for differences between the coupled and forced simulations (Brodeau et al., 2017), but seem to be of minor importance.

The spatial distribution of the coupling coefficients s_{st} obtained in the forced experiments $F_{\alpha=C1/4}$ and $F_{\alpha=C1/12}$ ~~, depicted in Fig. ?? and ??, mimic~~ reproduce the patterns of the coupled experiments ~~fairly closely. In particular, the spatial distributions~~ 10 ~~of the~~ with minor differences as shown for December to February (DJF) ~~mean~~ means (Fig. 11). We note larger s_{st} values in ~~both experiments C1/4 and $F_{\alpha=C1/4}$ show large negative values up to -3 in the Gulf Stream and Kuroshio regions as well as in the ACC. A notable deviation concerns the ACC region where the forced experiments tend to underestimate the~~ the ACC region by up to 0.9 and over the Kuroshio region in the coupled simulations. It is not clear why there is such a difference. As the relation between background winds and s_{st} ~~values obtained in the coupled experiments.~~ 15 ~~Mean of s_{st} DJF monthly values for (a) C1/4 and (c) $F_{\alpha=C1/4}$. Grey areas as in Fig. 2.~~ is not significant in large regions in the Southern Ocean it might be possible that in the coupled simulation other processes are also important for the surface stress calculation that are not captured in the forced simulations. Another possibility might be arising from differences in the bulk formulations (Brodeau et al., 2017).

A more quantitative comparison of the different experiments is given in Fig. 12, showing histograms of s_{st}. Both the absolute 20 and relative winds experiments do not compare well with the coupled experiments with global mean values of $s_{st}=-0.02$ ($F_{\alpha=0}$) and $s_{st}=-2.30$ ($F_{\alpha=1}$). Better results are given by the experiments where we estimated the α-values from the coupled
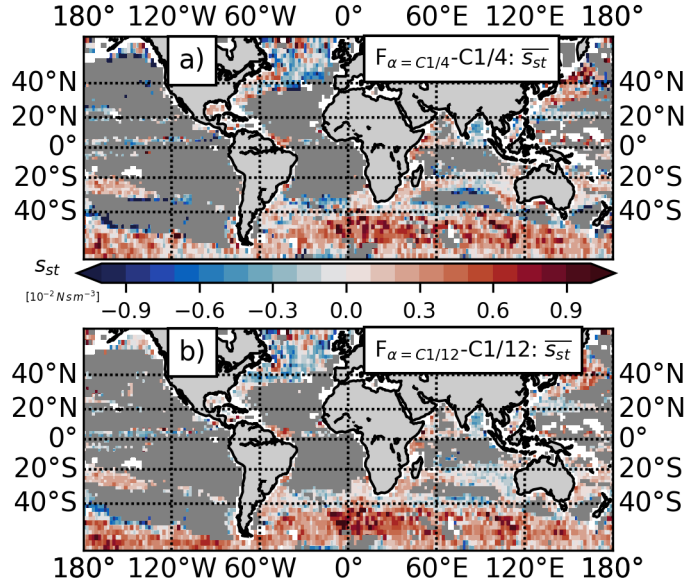
15

Figure 11. Mean of s_{st} ~~differences of~~ DJF monthly values for (a) ~~C1~~$F_{\alpha=C1/4}$-C1/~~12~~4 and (c) $F_{\alpha=C1/12}$-C1/12. Positive values means that the coupled simulations have stronger (more negative) s_{st} values. Grey areas defined as in Fig. 2.

experiments. While the global mean of s_{st} in $F_{\alpha=C1/4}$ (-1.53) are very close to the global mean of C1/4 (-1.51), for $F_{\alpha=C1/12}$ (-1.61) there is a slightly larger difference compared to C1/12 (-1.51). The distributions however show small differences: for s_{st} values between -2.25 and -1.5 the forced experiments have higher ~~PDE~~ probability density estimate when compared to the coupled experiments. It is likely that the differences in background winds are contributing to the differences in the distributions

5 (not shown).

This first assessment of the idea by *Renault et al.* (2016b) to modify the momentum flux formulation for forced ocean models to account for the re-energisation found in coupled shows that the relationship between the curl of the surface currents and the curl of the surface stress gets closer to the coupled model experiments when using the *Renault et al.* (2016b) approach. This

10 has implications for the ~~ocean simulation~~ simulated surface ocean in forced models and in particular for the energetics of the surface ocean. ~~Impacts on the surface EKE are discussed in the following section.~~
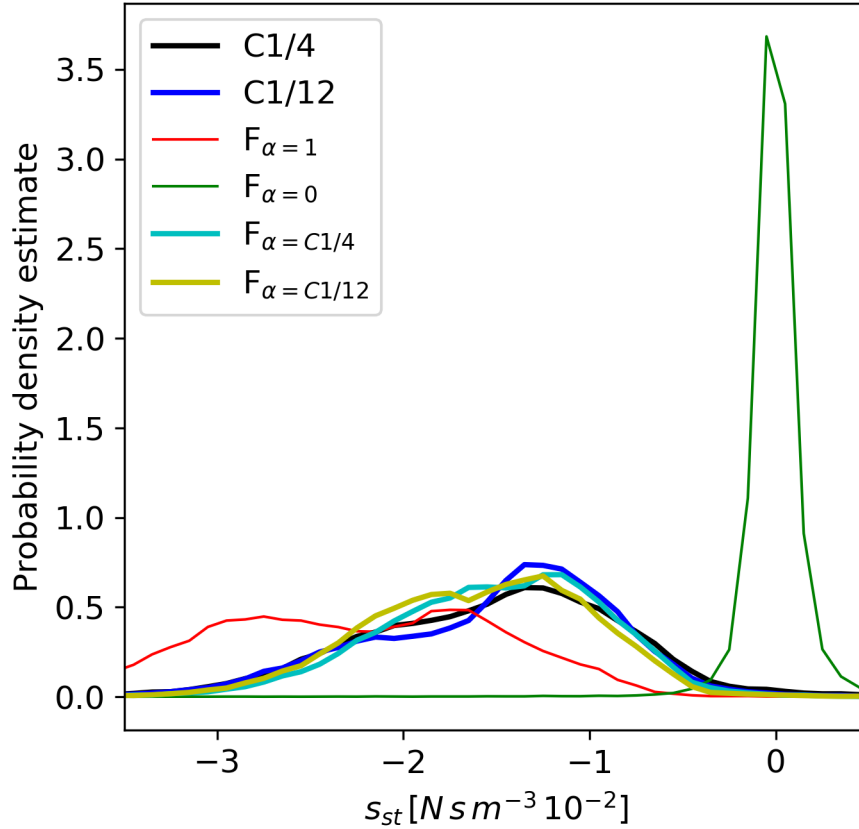
16

Figure 12. Normalized histogram (or probability density estimate) of ocean-surface current and surface stress coupling coefficient s_{st} for $2° \times 2°$ boxes from $60°$S to $60°$N (to exclude sea-ice regions~~; grey~~). Grey areas in Fig. 2 are excluded~~)~~.

3.4 ~~Assessment of impacts in a forced ocean model~~

The strength of the coupling between the curl of the ocean current and the curl of the surface stress (i.e., the choice of α) has implications for the ocean energetics. The part of the surface stress that is due to ocean surface currents acts as a damping mechanism for surface currents, hence for a larger α we expect to get a stronger damping, i.e., a weaker EKE. This is illustrated in Fig. 13a, by depicting the surface EKE (derived from the velocity deviations from annual mean velocity, based on time series of 5-day mean values) over the Gulf Stream. $F_{\alpha=1}$ ($F_{\alpha=0}$) produces the lowest (highest) level of EKE, while $F_{\alpha=C1/4}$ and $F_{\alpha=C1/12}$ lie in between, relatively, close to $F_{\alpha=1}$. A spatial view is given by a meridional section in the Pacific composed of a section through the Kuroshio Extension region at $218°$W and a section cutting through the equatorial and ACC region at $175°$W (Fig. 13 b). EKE levels are everywhere largest for $F_{\alpha=0}$ and smallest for $F_{\alpha=1}$, while $F_{\alpha=C1/4}$ and $F_{\alpha=C1/12}$ values
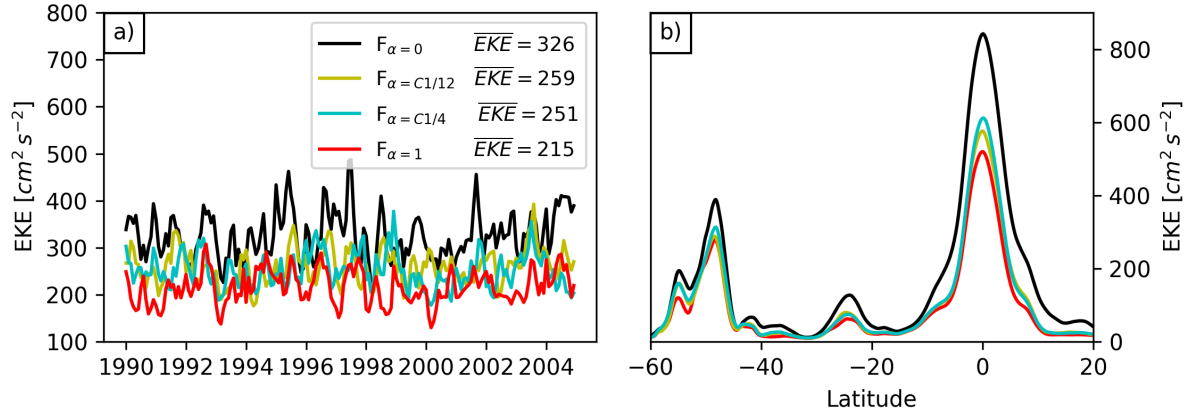
5

17

Figure 13. Surface eddy kinetic energy (EKE) for (a) the Gulf Stream (35-45°N, 37-75°W) and at (b) a meridional section through the ~~Kuroshio region (218°W) and through the~~ equatorial and ACC region ~~(at~~ 175°W ~~)~~(1990-2004 mean). Experiments shown are $F_{\alpha=0}$ (black), $F_{\alpha=1}$ (red), $F_{\alpha=C1/4}$ (green) and $F_{\alpha=C1/12}$ (yellow).

	$F_{\alpha=C1/4}$		$F_{\alpha=C1/12}$	
	EKE	MKE	EKE	MKE
ACC	6.3%	1.0%	6.3%	0.5%
Kuroshio	12.1%	1.6%	9.0%	5.2%
GSE	14.8%	-1.0%	16.5%	-1.2%
Eq. regions	13.6%	8.8%	11.8%	8.2%

Table 1. EKE and MKE change [%] with respect to $F_{\alpha=1}$ for the Antarctic Circumpolar Current (ACC, 70-45°S), Kuroshio (31-41°N, 140-157.5°E), Gulf Stream Extension (29-48.6°N, 37.5-83°W) and Equatorial regions (±5° off the equator).

lie in between. More specifically, regional ~~averages in EKE and mean kinetic energy (MKE) for $F_{\alpha=C1/4}$ ($F_{\alpha=C1/12}$) show increases by 6(6) and 1(1) in the ACC, 12(9) and 2(5)~~ changes of kinetic energy are large in the Kuroshio, ~~15(16) and -1(-1) in the Gulf Stream , and 14(12) and 9(8) in the equatorial region (±5° off the equator~~Gulf Stream and Equatorial regions and minor in the ACC (Tab. 1). A switch from relative to absolute winds shows even stronger changes in EKE and MKE. Direct
5   comparison of EKE to the coupled simulations is not meaningful here because differences in resolution and frequency of wind forcing (*Hughes and Wilson*, 2008; *Zhai et al.*, 2012) and details of the ocean configurations account for larger differences in EKE than the choice of α.

4 Discussion

In two coupled high resolution ocean models, we find a linkage between ocean surface currents and surface winds with pronounced spatio-temporal variability. The strength of the coupling coefficient s_w appears strongly affected by the atmospheric stability. The present results extend the findings of the regional model study of *Renault et al.* (2016b) to the global ocean-atmosphere system. By including this feedback in the bulk formulation of the momentum flux (1), with $\alpha = 1 - s_w$, using the spatially and temporally varying coefficient s_w estimated from the coupled models, the forced models appeared to capture the principal features of the coupling coefficient s_{st} for energetic oceanic regions. We want to point out that the improvement in the coupling coefficient s_{st} for forced models is quite important as it does show that the mechanical damping of surface currents is more realistic with respect to the coupled models. A first consequence of the 're-energisation tweak' is a slight, O(10%) increase in EKE and MKE for the energetic current regions compared to the 'relative wind' formulation used in current ocean modelling practice.

Renault et al. (2016b) found for the CCS, based on a similar methodology, coupling coefficients of $s_{st} = -1.2 \pm 0.35$ and $s_w = 0.23 \pm 0.1$ based on 5 year data from their coupled model. We find also for the CCS in the higher resolution version C1/12 similar estimates for the coupling coefficient for a 5 year period: $s_{st} = -1.26 \pm 0.13$ and $s_w = 0.28 \pm 0.04$. These findings are remarkably close given the differences in model setup and methodology.

We note several limitations of the method applied here: (1) For small curls of the ocean currents, the coupling coefficients appear to be biased, and cannot be robustly estimated (cf. Fig. A2). (2) The temporal and spatial scales of the atmosphere and ocean are not entirely separated. Therefore the results slightly vary with the cut-off length of the filter. (3) The results may depend on the parameterization of the vertical momentum flux in the atmospheric model. Further research should examine turbulence resolving atmospheric models, perhaps in conjunction with prescribed ocean currents, to understand how the state of the atmosphere modifies the response of near-surface winds in the presence of ocean currents.

The simulations presented here clearly show an imprint of the ocean surface currents on the surface stress and the near-surface winds. Estimates of surface stress (e.g., from scatterometer measurements) or the winds simulated in coupled simulations should thus be regarded as containing an imprint of the surface ocean state. Using either of these to drive an ocean-only model may have undesirable effects because it provides a spurious source of energy to the ocean model (*Xu and Scott*, 2008). On the other hand, in data sets produced for the forcing of ocean models (e.g. *Large and Yeager*, 2004; *Brodeau et al.*, 2010) winds are corrected by scatterometer derived winds only on larger scales for which the feedback from ocean surface currents should be small.

The present results support the proposition of *Renault et al.* (2016b) that the surface boundary condition for momentum in ocean-only simulations should include the surface current feedback to the wind. In contrast to a recent recommendation (*WCRP*, 2015) to use 'absolute winds' to avoid imprints of ocean currents in the wind/wind-stress, our results suggest using a revision of the 'relative winds'-formulation in the form of (1) with $\alpha = 1 - s_w$, ~~using~~ where a variable coefficient s_w is used in conjunction with winds from reanalysis products (where the atmosphere is forced only by SST) to force global ocean-sea ice

models. ~~The possibility of developing~~ Future research should be directed towards finding a reliable way to specify s_w.

The misrepresentation of damping of surface currents due to missing re-energization of near-surface winds is an important topic and needs to be explored in further studies. We suggest three major constitutive steps: (1) to study the re-energization of near-surface winds due to surface currents in uncoupled turbulence resolving atmospheric models, e.g. LES models and explore the possibility to develop a parameterization for s_w based on atmospheric state parameters ~~needs to be explored in further studies.~~; (2) to validate these results against the turbulence schemes as used in AGCMs; (3) when a parameterization of the re-energization effect is available, it could be tested in a sequence of global experiments involving fully coupled atmosphere-ocean models and uncoupled ocean models. The construction of a forcing data set for the uncoupled simulations needs very careful treatment in order to be as close to the atmosphere from the coupled system as possible. Such a set-up would allow to minimize errors that are due to differences in the forcing such as temporal and spatial resolution of wind and differences in bulk formulations.

5 Code availability

The plotting routines are available from https://github.com/RafaelAbel/current_feedback_on_winds

6 Data availability

The time and space variable α datasets are available from https://data.geomar.de/thredds/catalog/open_access/abel_et_al_2017_os/catalog.html

Appendix A: Energy spectra

An inspection of high-resolution coupled model output (Fig. A1) suggests an upper bound of about 200km for the transition between wavelengths where the atmosphere is more energetic and wavelengths where the ocean is more energetic. We find that this scale separation is sometimes more pronounced and in some regions not even valid and show this ~~exemplarily for three locations~~ exemplary for three regions: in a large box in the South Pacific, the atmospheric velocity spectral density dominates at all scales; in a rather small box in the North Pacific, we find a transition from atmospheric domination to oceanic domination at wavelengths of about 200km; in the Gulf Stream Extension, below wavelengths of 150km, atmospheric and oceanic velocity spectral densities are at the same level. As we are attempting to find a signal that is imprinted by the ocean on the atmosphere we need to consider energetic regions of the ocean. With conditions such as in the South Pacific, we will not be able to detect the oceanic imprint (discussed in Appendix B).
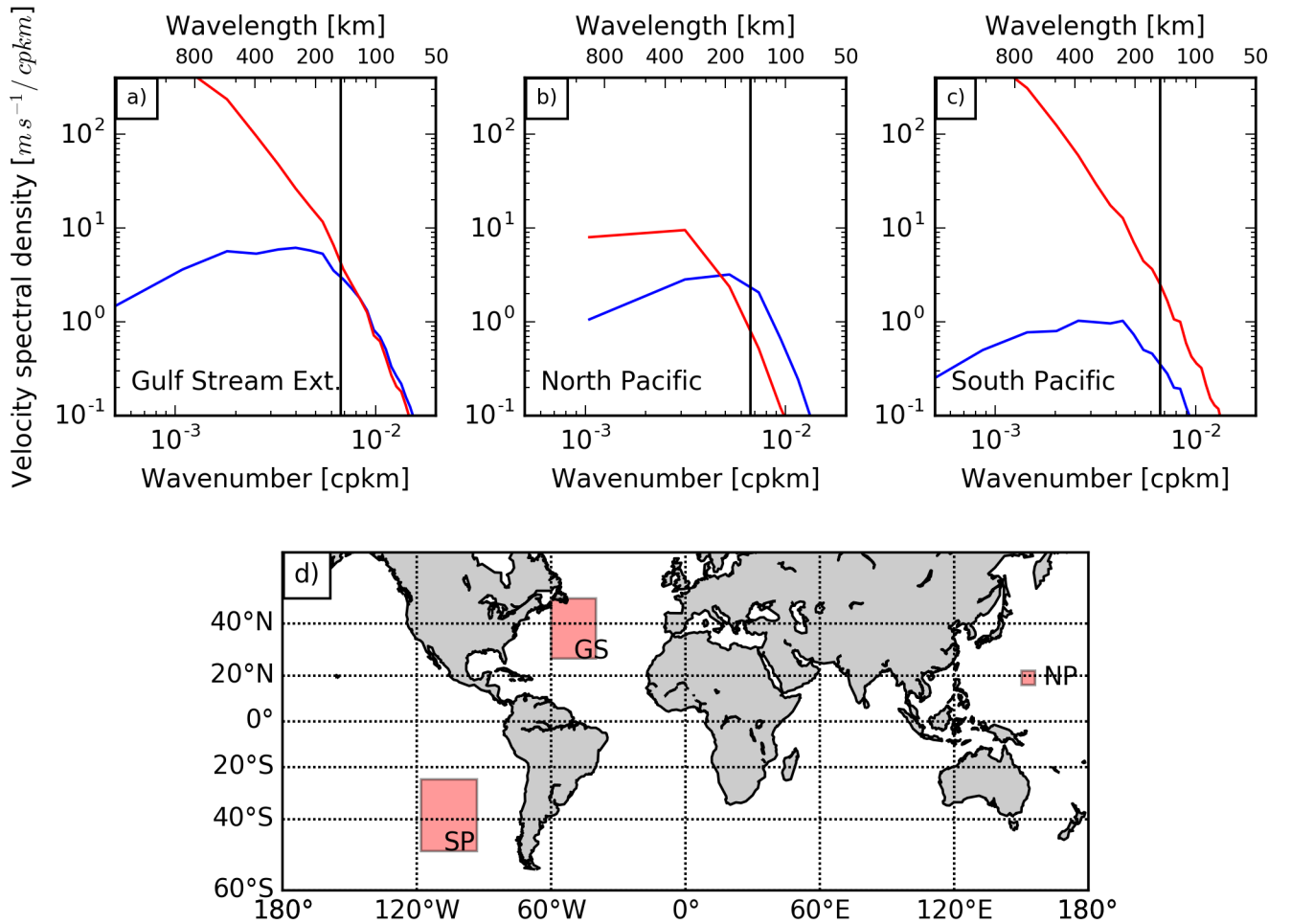
Figure A1. Isotropic wavenumber spectra of ocean velocity (blue) and wind speed (red) for (a) South Pacific, (b) North Pacific and (c) Gulf Stream Extension in C1/4 monthly output. In d) you find the exact positions of the boxes. Vertical black lines represent the 150km wavelength to illustrate the cutoff length of the high-pass filter used for this study. The idea of using a high-pass filter is to exclude wavelengths where atmospheric variability is larger than oceanic. We see in the north Pacific (b) that at higher wavenumbers oceanic spectral density is larger that atmospheric and in the Gulf Stream Extension (c) they have the same order of magnitude. The 150km high-pass filter seems to be a good choice for the North Pacific box and for the Gulf Stream Extension box. In the South Pacific atmospheric variability dominates at all wavenumbers. This is also a region where we were not able to estimate coupling coefficients (see Fig 2).

Appendix B: Biased scatter plots

As seen in Fig. 1 the relationship between ~~curl(u) and curl(wind)~~ $curl(u)$ and $curl(wind)$ does not follow exactly the suggested linear fit. This becomes particularly problematic if curl(u), i.e. the spread along the x-axis, is relatively small. With small ~~curl(u)~~ $curl(u)$ the estimation of the slope of the linear regression tends to be biased towards large values. This can be seen when mapping the maximum difference between ~~curl(u)~~ $curl(u)$ values to the estimated s_w (Fig. A2). There we see that s_w and $\sigma(s_w)$ get large if $|curl(u)| < 1$. We choose to ignore these values and mark them as grey areas in the figures with global maps.

Appendix C: Degrees of Freedom estimation

The standard error of the slope of the linear regression is estimated by:

$$SE = \sqrt{\frac{SS_y/SS_x - b^2}{DOF}}, \tag{C1}$$

where $SS_y = \sum(y_i - \bar{y}_i)^2$, $SS_y = \sum(x_i - \bar{x}_i)^2$, $\bar{}$ denotes mean, b is slope of linear regression and DOF are the degrees of freedom (DOF).

Given any three dimensional data set (two space and one time dimension) there will be coherence, meaning that time and space points can be dependent on each other. Therefore the DOF estimation needs to consider both temporal and spatial DOF. For the temporal DOF of freedom we follow *Bretherton et al.* (1999), estimating the ratio of effective sample size (ESS, N^*) to sample size N

$$N^*/N = \frac{1 - r_1 r_2}{1 + r_1 r_2}, \tag{C2}$$

while $r_{1,2}$ is the lag-one autocorrelation for dataset 1,2. If only one dataset is used $r_1 = r_2$. For the spatial DOF estimation we use an adapted binomial method (B-method) of *Livezey and Chen* (1983) and *Wang and Shen* (1999), where a random time series is correlated with every spatial point since by chance some points will give a significant correlation with that random time series, the points with significant correlation share coherence, which is exploited to estimate the coherence of the field. To estimate the total DOF of the given three-dimensional (with two spatial and one temporal dimension t) climate data set we combine the spatial (DOF_S) and temporal DOF estimation

$$DOF_{total} = DOF_S \cdot t \cdot N^*/N \tag{C3}$$

Details of the estimation and a python-based program can be found at https://github.com/RafaelAbel/DOF_estimation.

Appendix D: Model vertical levels

Here we give a reduced list of the vertical levels of the atmospheric model. For a full list of the vertical levels we refer readers to Walters et al. (2017).
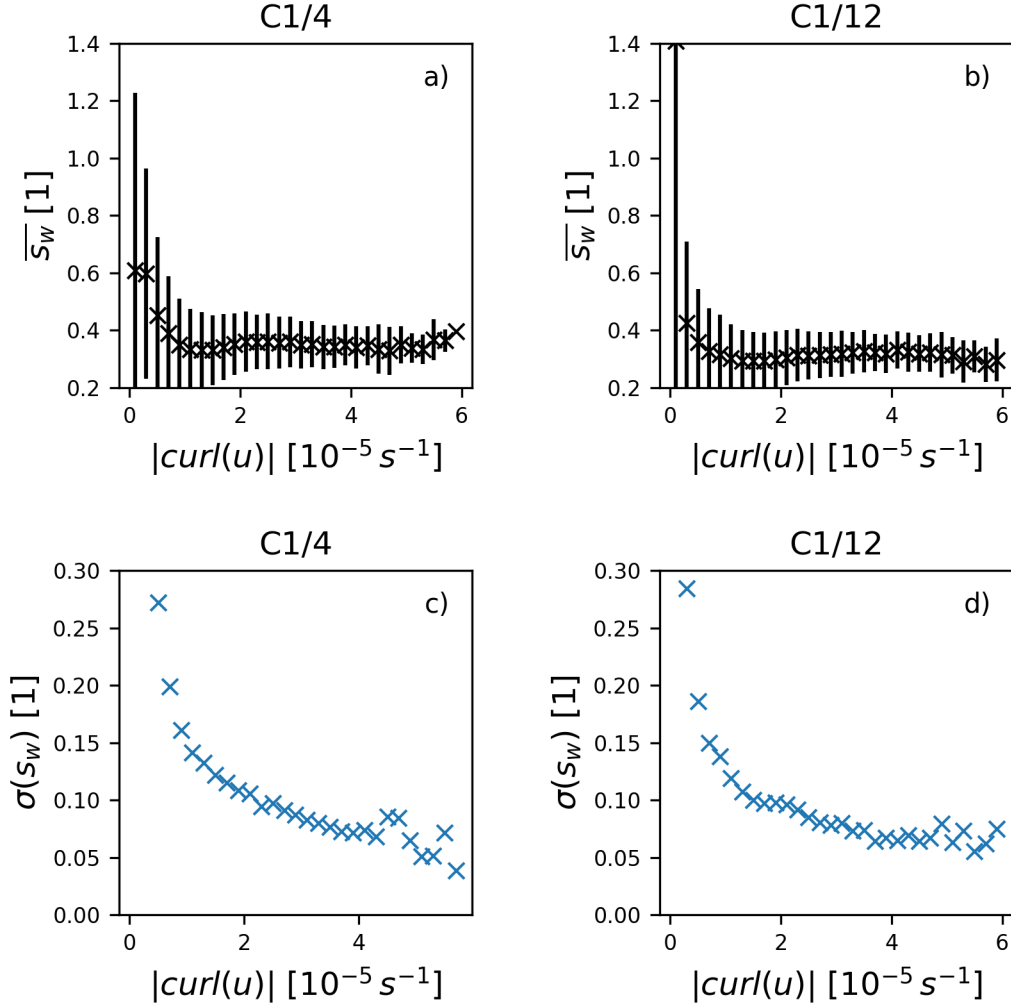
Figure A2. Coupling coefficient s_w as a function of absolute value of curl(u) for (a) C1/4, (b) C1/12 and standard deviation of s_w for (c) C1/4, (d) C1/12. For small $|curl(u)|$ s_w and $\sigma(s_w)$ get larger. We see this as a problem of the method and therefore neglect values where range $|curl(u)| < 1$. Similar behaviour is seen for s_{st} and neglected as well. This results in the grey areas in Fig. 2, 5 and 9.

Level	Height (m)
1	10.00
10	730.00
20	2796.67
30	6196.67
40	10930.12
50	17012.40
60	24710.70
70	35927.89
80	58978.35
85	82050.01

Table 2. Reduced list of the total 85 vertical levels in the atmospheric model GA6.

References

Antonov, J., Levitus, S., Boyer, T., Conkright, M., O'Brien, T., and Stephens, C. (1998), World Ocean Atlas 1998 Vol. 1: Temperature of the Atlantic Ocean NOAA Atlas NESDIS 27,, *U.S. Government Printing Office*, Washington, D.C, 1998

Boyer, T., Levitus, S., Antonov, J., Conkright, M., O'Brien, T., and Stephens, C. (1998), World Ocean Atlas 1998 Vol. 4: Salinity of the Atlantic Ocean NOAA Atlas NESDIS 30,, *U.S. Government Printing Office*, Washington, D.C, 1998

Bretherton, C. S., M. Widmann, V. P. Dymnikov, J. M. Wallace, and I. Bladé (1999), The effective number of spatial degrees of freedom of a time-varying field, *J. Clim.*, *12*(7), 1990–2009, doi:10.1175/1520-0442(1999)012<1990:TENOSD>2.0.CO;2.

Brodeau, L., B. Barnier, A.-M. Treguier, T. Penduff, and S. Gulev (2010), An ERA40-based atmospheric forcing for global ocean circulation models, *Ocean Model.*, *31*(3-4), 88–104, doi:10.1016/j.ocemod.2009.10.005.

Brodeau, L., Barnier, B., Gulev, S. K., and Woods, C.: Climatologically Significant Effects of Some Approximations in the Bulk Parameterizations of Turbulent Air-Sea Fluxes, J. Phys. Oceanogr., 47, 5–28, doi:10.1175/JPO-D-16-0169.1, http://journals.ametsoc.org/doi/10.1175/JPO-D-16-0169.1, 2017.

Bryan, F. O., R. Tomas, J. M. Dennis, D. B. Chelton, N. G. Loeb, and J. L. Mcclean (2010), Frontal scale air-sea interaction in high-resolution coupled climate models, *J. Clim.*, *23*(23), 6277–6291, doi:10.1175/2010JCLI3665.1.

Byrne, D., M. Munnich, I. Frenger, and N. Gruber (2016), Mesoscale atmosphere ocean coupling enhances the transfer of wind energy into the ocean, *Nat. Commun.*, (May), 1–8, doi:10.1038/ncomms11867.

Chelton, D. B., M. G. Schlax, M. H. Freilich, and R. F. Milliff (2004), Satellite measurements reveal persistent small-scale features in ocean winds., *Science*, *303*(5660), 978–83, doi:10.1126/science.1091901.

Chelton, D. B., M. G. Schlax, and R. M. Samelson (2007), Summertime Coupling between Sea Surface Temperature and Wind Stress in the California Current System, *J. Phys. Oceanogr.*, *37*(3), 495–517, doi:10.1175/JPO3025.1.

Dewar, W. K., and G. R. Flierl (1987), Some Effects of the Wind on Rings, *J.Phys. Oceanogr.*, *17*, 1653-67, doi:10.1175/1520-0485(1987)017.

Duhaut, T., and D. Straub (2006), Wind Stress Dependence on Ocean Surface Velocity: Implications for Mechanical Energy Input to Ocean Circulation, *J. Phys. Oceanogr.*, *36*, 202–211, doi:10.1175/JPO2842.1.

Eden, C., and H. Dietze (2009), Effects of mesoscale eddy/wind interactions on biological new production and eddy kinetic energy, *J. Geophys. Res.*, *114*(C5), C05,023, doi:10.1029/2008JC005129.

Frenger, I., N. Gruber, R. Knutti, and M. Münnich (2013), Imprint of Southern Ocean eddies on winds, clouds and rainfall, *Nat. Geosci.*, *6*(8), 608–612, doi:10.1038/ngeo1863.

Griffies, S. M., A. Biastoch, C. Böning, F. Bryan, G. Danabasoglu, E. P. Chassignet, M. H. England, R. Gerdes, H. Haak, R. W. Hallberg, W. Hazeleger, J. Jungclaus, W. G. Large, G. Madec, A. Pirani, B. L. Samuels, M. Scheinert, A. S. Gupta, C. a. Severijns, H. L. Simmons, A. M. Treguier, M. Winton, S. Yeager, and J. Yin (2009), Coordinated Ocean-ice Reference Experiments (COREs), *Ocean Model.*, *26*(1-2), 1–46, doi:10.1016/j.ocemod.2008.08.007.

Hewitt, H. T., M. J. Roberts, P. Hyder, T. Graham, J. Rae, S. E. Belcher, R. Bourdalle-Badie, D. Copsey, A. Coward, C. Guiavarch, C. Harris, R. Hill, J. J.-M. Hirschi, G. Madec, M. S. Mizielinski, E. Neininger, A. L. New, J.-C. Rioual, B. Sinha, D. Storkey, A. Shelly, L. Thorpe, and R. A. Wood (2016), The impact of resolving the Rossby radius at mid-latitudes in the ocean: results from a high-resolution version of the Met Office GC2 coupled model, *Geosci. Model Dev. Discuss.*, (April), 1–35, doi:10.5194/gmd-2016-87.

Hughes, C. W., and C. Wilson (2008), Wind work on the geostrophic ocean circulation: An observational study of the effect of small scales in the wind stress, *J. Geophys. Res.*, *113*(C2), 1–10, doi:10.1029/2007JC004371.

Hutchinson, D. K., A. M. C. Hogg, and J. R. Blundell (2010), Southern Ocean Response to Relative Velocity Wind Stress Forcing, *J. Phys. Oceanogr.*, *40*(2), 326–339, doi:10.1175/2009JPO4240.1.

Large, W., and S. Yeager (2004), Diurnal to Decadal Global Forcing For Ocean and Sea-Ice Models : The Data Sets and Flux Climatologies, NCAR Technical Note NCAR/TN-460+STR, doi:10.5065/D6KK98Q6

Large, W. G., and S. G. Yeager (2009), The global climatology of an interannually varying air-sea flux data set, *Clim. Dyn.*, *33*(2-3), 341–364, doi:10.1007/s00382-008-0441-3.

Livezey, R. E., and W. Y. Chen (1983), Statistical Field Significance and its Determination by Monte Carlo Techniques, *Mon. Weather Rev.*, *111*(1), 46–59, doi:10.1175/1520-0493(1983)111<0046:SFSAID>2.0.CO;2.

Luo, J.-J., S. Masson, E. Roeckner, G. Madec, T. Yamagata, and P. Science (2004), Reducing Climatology Bias in an Ocean - Atmosphere CGCM with Improved, *J. Clim.*, *18*, 2344–2360, doi:10.1175/JCLI3404.1.

Ma, X., Z. Jing, P. Chang, X. Liu, R. Montuoro, R. J. Small, F. O. Bryan, R. J. Greatbatch, P. Brandt, D. Wu, X. Lin, and L. Wu (2016), Western boundary currents regulated by interaction between ocean eddies and the atmosphere, *Nature*, *535*(7613), 533–537, doi:10.1038/nature18640.

Madec, G. (2011), *NEMO ocean engine*, 27, tech. rep. ed., Inst. Pierre-Simon Laplace (IPSL), France.

Mantua, N. J., Hare, S. R., Zhang, Y., Wallace, J. M., and Francis, R. C.: A Pacific interdecadal climate oscillation with impacts on salmon production, Bull. Amer. Meteor. Soc., 78, 1069–1079, 1997.

Minobe, S., A. Kuwano-Yoshida, N. Komori, S.-P. Xie, and R. J. Small (2008), Influence of the Gulf Stream on the troposphere., *Nature*, *452*(7184), 206–9, doi:10.1038/nature06690.

Moulin, A., and A. Wirth (2016), Momentum Transfer Between an Atmospheric and an Oceanic Layer at the Synoptic and the Mesoscale: An Idealized Numerical Study, *Boundary-Layer Meteorol.*, pp. 1–18, doi:10.1007/s10546-016-0153-x.

Okumura, Y., Xie, S. P., Numaguti, A., and Tanimoto, Y.: Tropical Atlantic air-sea interaction and its influence on the NAO, Geophysical Research Letters, 28, 1507–1510, doi:10.1029/2000GL012565, 2001.

Pacanowski, R. C. (1987), Effect of Equatorial Currents on Surface Stress, *J. Phys. Oceanogr.*, *17*, 833–838, doi:10.1175/1520-0485(1987)017.

Perlin, N., E. D. Skyllingstad, R. M. Samelson, and P. L. Barbour (2007), Numerical Simulation of Air-Sea Coupling during Coastal Upwelling, *J. Phys. Oceanogr.*, *37*(8), 2081–2093, doi:10.1175/JPO3104.1.

Rath, W., R. J. Greatbatch, and X. Zhai (2013), Reduction of near-inertial energy through the dependence of wind stress on the ocean-surface velocity, *J. Phys. Ocean.*, *118*(6), 2761–2773, doi:10.1002/jgrc.20198.

Renault, L., A. Hall, and J. C. McWilliams (2016a), Orographic shaping of US West Coast wind profiles during the upwelling season, *Clim. Dyn.*, pp. 1–17, doi:10.1007/s00382-015-2583-4.

Renault, L., M. J. Molemaker, J. C. McWilliams, A. F. Shchepetkin, F. Lemarié, D. Chelton, S. Illig, and A. Hall (2016b), Modulation of Wind-Work by Oceanic Current Interaction with the Atmosphere, *J. Clim.*, pp. 0–52, doi:10.1175/JPO-D-15-0232.1.

Renault, L., Molemaker, M. J., Gula, J., Masson, S., and McWilliams, J. C.: Control and Stabilization of the Gulf Stream by Oceanic Current Interaction with the Atmosphere, Journal of Physical Oceanography, 46, 3439–3453, doi:10.1175/JPO-D-16-0115.1, http://journals.ametsoc.org/doi/10.1175/JPO-D-16-0115.1, 2016.

Roberts, M. J., H. T. Hewitt, P. Hyder, D. Ferreira, S. A. Josey, M. Mizielinski, and A. Shelly (2016), Impact of ocean resolution on coupled air-sea fluxes and large-scale climate, *Geophys. Res. Lett.*, doi:10.1002/2016GL070559.

Samelson, R. M., E. D. Skyllingstad, D. B. Chelton, S. K. Esbensen, L. W. O'Neill, and N. Thum (2006), On the coupling of wind stress and sea surface temperature, *J. Clim.*, *19*(8), 1557–1566, doi:10.1175/JCLI3682.1.

5 Scott, R. B., and Y. Xu (2009), An update on the wind power input to the surface geostrophic flow of the World Ocean, *Deep. Res. Part I Oceanogr. Res. Pap.*, *56*(3), 295–304, doi:10.1016/j.dsr.2008.09.010.

Seo, H., A. J. Miller, and J. R. Norris (2016), Eddy-wind interaction in the California Current System: dynamics and impacts, *J. Phys. Oceanogr.*, (1989), 151130150615,002, doi:10.1175/JPO-D-15-0086.1.

Shuckburgh, E., G. Maze, D. Ferreira, J. Marshall, H. Jones, and C. Hill (2011), Mixed Layer Lateral Eddy Fluxes Mediated by Air-Sea
10 Interaction, *J. Phys. Oceanogr.*, *41*(1), 130–144, doi:10.1175/2010JPO4429.1.

Small, R., S. DeSzoeke, S. Xie, L. O'Neill, H. Seo, Q. Song, P. Cornillon, M. Spall, and S. Minobe (2008), Air-sea interaction over ocean fronts and eddies, *Dyn. Atmos. Ocean.*, *45*(3-4), 274–319, doi:10.1016/j.dynatmoce.2008.01.001.

Smith, S. D. (1988), Coefficients for sea surface wind stress, heat flux, and wind profiles as a function of wind speed and temperature, *J. Geophys. Res. Ocean.*, *93*(C12), 15,467–15,472, doi:10.1029/JC093iC12p15467.

15 Spall, M. a. (2007), Midlatitude Wind Stress-Sea Surface Temperature Coupling in the Vicinity of Oceanic Fronts, *J. Clim.*, *20*(15), 3785–3801, doi:10.1175/JCLI4234.1.

Wallace, J. M., T. P. Mitchell, and C. Deser (1989), The Influence of Sea-Surface Temperature on Surface Wind in the Eastern Equatorial Pacific: Seasonal and Interannual Variability, doi:10.1175/1520-0442(1989)002<1492:TIOSST>2.0.CO;2.

Walters, D., Boutle, I., Brooks, M., Melvin, T., Stratton, R., Vosper, S., Wells, H., Williams, K., Wood, N., Allen, T., Bushell, A., Copsey, D.,
20 Earnshaw, P., Edwards, J., Gross, M., Hardiman, S., Harris, C., Heming, J., Klingaman, N., Levine, R., Manners, J., Martin, G., Milton, S., Mittermaier, M., Morcrette, C., Riddick, T., Roberts, M., Sanchez, C., Selwood, P., Stirling, A., Smith, C., Suri, D., Tennant, W., Luigi Vidale, P., Wilkinson, J., Willett, M., Woolnough, S., and Xavier, P.: The Met Office Unified Model Global Atmosphere 6.0/6.1 and JULES Global Land 6.0/6.1 configurations, Geosci. Model Dev., 10, 1487–1520, doi:10.5194/gmd-10-1487-2017, 2017.

Wang, X., and S. S. Shen (1999), Estimation of spatial degrees of freedom of a climate field, *J. Clim.*, *12*(5 I), 1280–1291, doi:10.1175/1520-
25 0442(1999)012<1280:EOSDOF>2.0.CO;2.

WCRP (2015), CLIVAR Ocean Model Development Panel (OMDP) mini workshop on forcing ocean and sea-ice models, *WCRP Rep. 9, CLIVAR Rep. 202, 22pp.* [Available online at http://www.clivar.org/sites/default/files/documents/OMDP_Grenoble_report.pdf]

Xie, S. P. (2004), Satellite observations of cool ocean-atmosphere interaction, *Bull. Am. Meteorol. Soc.*, *85*(2), 195–208, doi:10.1175/BAMS-85-2-195.

30 Xu, Y., and R. B. Scott (2008), Subtleties in forcing eddy resolving ocean models with satellite wind data, *Ocean Model.*, *20*(3), 240–251, doi:10.1016/j.ocemod.2007.09.003.

Xu, C., Zhai, X., and Shang, X.-d.: Work done by atmospheric winds on mesoscale, Journal of Geophysical Research : Oceans, pp. 1–7, doi:10.1002/2016GL071275.1., 2016.

Zhai, X., and R. J. Greatbatch (2007), Wind work in a model of the northwest Atlantic Ocean, *Geophys. Res. Lett.*, *34*(4), 1–4,
35 doi:10.1029/2006GL028907.

Zhai, X., H. L. Johnson, D. P. Marshall, and C. Wunsch (2012), On the Wind Power Input to the Ocean General Circulation, *J. Phys. Oceanogr.*, *42*(8), 1357–1365, doi:10.1175/JPO-D-12-09.1.